

SPURIOUS CURRENTS IN A FINITE-ELEMENT BASED LEVEL SET METHOD FOR TWO PHASE FLOW

Sara Zahedi,^{*} Martin Kronbichler,[†] Gunilla Kreiss[‡]

Abstract

A study of spurious currents in finite element based simulations of the incompressible Navier–Stokes equations for two phase flows is presented, based on computations on a circular drop in equilibrium. The interface is accounted for by a level set method. It is shown that a sharp surface tension force, expressed as a line integral along the interface, can give rise to large spurious currents and oscillations in the pressure. If instead a regularized surface tension representation is used, exact force balance at the interface is possible, both for a fully coupled discretization approach as well as for a fractional step projection method. We illustrate that with exact force balance, the spurious currents are of the order of the tolerance of the linear solver. However, the numerical curvature calculation introduces errors, that cause spurious currents. Different ways to extend the curvature from the interface to the whole domain are discussed and investigated. It is shown that the choice of curvature extension has a significant impact on the error in pressure. The impact of using different finite element spaces is also investigated.

Key words level set method, spurious currents, two phase flow, finite element method

1 Introduction

Multiphase flow simulation is an important tool for predicting and controlling technical systems in a wide range of industrial applications. Examples include liquid phase sintering and inkjet printing. In order to improve the quality of the

^{*}School of Computer Science and Communication, KTH Royal Institute of Technology, SE-100 44 Stockholm, Sweden, sara7@kth.se. Corresponding author.

[†]Division of Scientific Computing, Uppsala University, P.O. Box 337, SE-751 05 Uppsala, Sweden, martin.kronbichler@it.uu.se.

[‡]Division of Scientific Computing, Uppsala University, P.O. Box 337, SE-751 05 Uppsala, Sweden, gunilla.kreiss@it.uu.se.

simulation, accurate numerical models need to be developed. The representation of the singular surface tension forces acting at interfaces separating immiscible fluids, the discontinuous pressure, and the jump in the fluid densities and viscosities pose challenges on the numerical methods. Moreover, it is important to accurately represent the interfaces separating the different fluids.

For fixed-grid flow solvers where a predefined grid is used to describe the velocity field, interface representation techniques can essentially be divided into two classes. In the first class, interfaces are represented explicitly; the interface can for example be defined by the use of so-called marker particles that track the interface. Examples include the immersed boundary method [1] and the front-tracking method [2]. In the second class, the interface is instead represented implicitly by a function defined on a higher dimension than the interface. The level set method [3], the volume-of-fluid method [4], and the phase field method [5] are examples of methods based on this concept. Compared to methods in which the interface is explicitly tracked, these methods handle topological changes – such as merging and breaking – more easily. Both classes of interface representation techniques can provide accurate representation and advection of the interfaces.

Taking surface tension into account leads to a jump condition for the normal stress at the interface. A common strategy in fixed-grid methods is to include the jump conditions in the model by adding a singular source term to the Navier-Stokes equations [1, 6, 7]. In the continuum surface force model the forces due to surface tension are expressed in terms of Dirac delta functions with support on the interfaces. Numerically, delta functions can be approximated by regularized discrete operators that distribute the force over a band near the interface. In level set methods, care is needed when regularized delta functions are used since only certain delta function approximations converge as the mesh is refined [8, 9]. An alternative to the continuum surface force model is to directly impose the jump conditions at the interface. Within the context of finite differences, an example is the ghost fluid method [10]. In the finite element framework, a line integral added to the equations of motion [11] needs to be evaluated. These approaches obviate any discrete representation of delta functions. However, accurate representation of interfacial jump conditions remains a difficult issue for fixed-grid methods.

Many researchers have observed unphysical flows close to the interface in multiphase flow simulations [12, 13, 14]. These unphysical flows are referred to as parasitic flows or spurious currents, and have been observed both with explicit and implicit representations of the interface, and with different representations of the surface tension. Lafaurie et al. concluded from numerical experiments that the magnitude of the spurious currents scaled with the inverse of the capillary number [12]. Spurious currents can lead to unphysical movements of the interface and thus misinterpretations of the flow physics. At high Reynolds numbers spurious currents may grow and destroy the interface [14]. In [13] it was

shown using a volume of fluid method and the continuum surface force model that the spurious currents may not decrease with mesh refinement.

The appearance of spurious currents is well illustrated by simulation of a drop in equilibrium without gravity. In this case the pressure is given by Laplace's formula and the velocity is zero. However, imbalances between the discrete representation of capillary forces and the pressure jump across the interface create a nonzero velocity field near the interface. Numerous variants of surface tension force representations and improvements of the curvature computation have been presented in order to reduce the spurious currents, see for example [13, 15, 16, 17, 18]. Most of those studies focus on flow solvers using finite difference and finite volume discretizations. However, finite element discretizations are becoming increasingly popular since the finite element framework allows for easy implementation of adaptive mesh refinement and representation of complex geometries without substantial implementation hurdles.

In this paper, we study spurious currents in finite element based methods for capillary dominated two-phase flow. The interface is represented by the conservative level set method presented in [19]. Compared to the standard level set method, see for example [20, 21], this representation has the advantage that good area conservation can be obtained but the computation of accurate normals and curvature is more difficult. For the Navier–Stokes equations we consider a fully coupled and a fractional step projection method. We use either a sharp representation of the surface tension [11] or a regularized surface tension force.

The outline of this article is as follows. In Section 2, we review the conservative level set model for two-phase flow in the continuous setting. Section 3 discusses finite element discretizations of the model. In Section 4, we study a drop in equilibrium and investigate how spurious currents depend on the capillary number, the spatial mesh size, the time step, the interface thickness, the balance between the discrete representation of the forces, the finite element spaces, and the evaluation of the curvature. We summarize our results in Section 5.

2 The mathematical description

The motion of two incompressible immiscible fluids is given by the incompressible Navier–Stokes equations, coupled to an equation that models the evolution of the interface.

2.1 The governing equations of fluid flow

Assume that a given domain Ω is occupied by two incompressible immiscible fluids separated by an interface Γ . The two subdomains containing the fluids are denoted by Ω_1 and Ω_2 , see Fig. 1. We assume that the interface is not in contact with the boundary of the domain $\partial\Omega$. The standard model for each domain

(Ω_1 and Ω_2) is the time dependent incompressible Navier–Stokes equations with boundary conditions at the interface Γ [22]. Surface tension effects leads to a jump condition for the normal stress at the interface. The velocity field is continuous across the interface. In this paper, however, we solve the Navier–Stokes equations in the whole domain Ω and include the effect of surface tension by adding a singular source term to the equations. In non-dimensional form, the Navier–Stokes equations read:

$$\begin{aligned} \partial_t(\rho\mathbf{u}) + \nabla \cdot (\rho\mathbf{u}\mathbf{u}) &= -\nabla p + \frac{1}{\text{Re}} \nabla \cdot (2\mu\nabla^s\mathbf{u}) + \frac{1}{\text{Fr}^2} \rho \mathbf{e}_g + \frac{1}{\text{ReCa}} \kappa \mathbf{n} \delta_\Gamma, \\ \nabla \cdot \mathbf{u} &= 0. \end{aligned} \quad (1)$$

Here \mathbf{u} , p , ρ , and μ denote velocity, pressure, density, and viscosity, respectively. In general, ρ and μ are discontinuous across the interface separating the two fluids. Throughout this paper we use dimensionless viscosity $\mu_1 = \mu_2 = 1$ and density $\rho_1 = \rho_2 = 1$. The quantity $\nabla^s\mathbf{u} = \frac{1}{2}(\nabla\mathbf{u} + (\nabla\mathbf{u})^T)$ denotes the viscous stress tensor. The curvature and normal of the interface Γ are denoted by κ and \mathbf{n} , and δ_Γ is a Dirac delta measure with support on Γ . Its action on any smooth test function v is given by

$$\int_\Omega \delta_\Gamma v d\Omega = \int_\Gamma v d\Gamma. \quad (2)$$

We denote by \mathbf{e}_g the direction of gravity and by g the gravitational acceleration. The dimensionless Reynolds, capillary, and Froude numbers, are given by

$$\text{Re} = \frac{\rho_{\text{ref}} u_{\text{ref}} l_{\text{ref}}}{\mu_{\text{ref}}}, \quad \text{Ca} = \frac{\mu_{\text{ref}} u_{\text{ref}}}{\sigma}, \quad \text{and} \quad \text{Fr} = \frac{u_{\text{ref}}}{\sqrt{l_{\text{ref}} g}}, \quad (3)$$

respectively. The parameter σ is the surface tension coefficient. The Weber number is defined as

$$\text{We} = \text{Re} \cdot \text{Ca}. \quad (4)$$

In this paper, we use no–slip boundary conditions for the velocity and fix the pressure to be zero at an arbitrary point on the boundary. We prescribe a divergence-free initial velocity field $\mathbf{u}(\cdot, 0) = \mathbf{u}_0$ and the initial position of the interface Γ . The interface is transported by the local fluid speed. The representation of the interface and a model for its motion will be described in the next section.

2.2 A level set representation of the interface

We use the conservative level set method of [19] to represent the interface. Instead of the signed distance function that is often used to define the interface [21, 20], this method uses a regularized indicator function Φ . The indicator function takes the value 0 in one fluid and the value 1 in the other fluid. The 0.5–level set of the regularized indicator function Φ defines the interface.

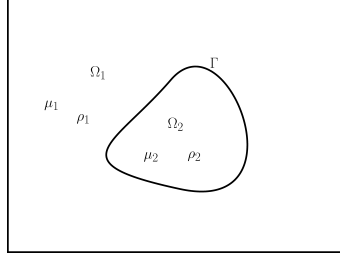


Figure 1: The domain $\Omega \in \mathbb{R}^2$ is occupied by two immiscible fluids separated by an interface Γ . The domains occupied by the fluids are denoted Ω_1 and Ω_2 . Here $\Gamma \cap \partial\Omega = \emptyset$. Density is denoted by ρ and viscosity by μ .

The level set function is initialized as

$$\Phi_0(x, y) = \frac{1}{1 + e^{-\frac{d(x,y)}{\varepsilon}}}, \quad (5)$$

where $d(x, y)$ is the signed distance function to the interface. To evolve the interface, we solve the advection equation for the level set function Φ ,

$$\Phi_t + \nabla \cdot (\Phi \mathbf{u}) = 0, \quad \Phi(\cdot, 0) = \Phi_0. \quad (6)$$

The shape of the regularized indicator function is maintained by a reinitialization procedure applied in each time step. The reinitialization is modeled by the partial differential equation

$$\Phi_t + \nabla \cdot (\Phi(1 - \Phi)\mathbf{n}) - \nabla \cdot (\varepsilon(\nabla\Phi \cdot \mathbf{n})\mathbf{n}) = 0, \quad (7)$$

where a non-linear convection term in the normal direction is balanced by normal diffusion. The normal vector field \mathbf{n} is defined as

$$\mathbf{n} = \frac{\nabla\Phi}{|\nabla\Phi|}. \quad (8)$$

The desired shape of Φ is obtained by solving equation (7) to steady state. The parameter ε controls the amount of diffusion in the normal direction and thereby the thickness of the interface. In order to obtain accurate results, the parameter ε should be smaller than typical geometrical features of the interface. It is essential for the conservation of mass of the individual fluids to use no-flux boundary conditions for Φ except at in- or outflow boundaries, combined with conservative numerical discretizations of the advection equation (6) and the reinitialization equation (7).

3 The computational models

We discretize the Navier–Stokes equations described in equation (1) using two different continuous finite element based methods. The first method is fully implicit in time and a coupled system for the velocity, pressure and the level set function is solved, hereinafter *the coupled method*. In the second method a fractional step projection method is used. This decouples the equations for velocity and pressure, hereinafter *the decoupled method*.

The interface is evolved by solving the advection equation (6) and then the reinitialization equation described in equation (7) to steady state. In the coupled method a second order backward difference formula BDF-2 is used for the time discretization in the advection equation. While the first order backward Euler formula is used in the decoupled method. For the discretization of the reinitialization equation we refer to [19]. Usually two reinitialization steps are required.

3.1 The evaluation of the surface tension force

As noted in Section 2.1, the surface tension effect is treated as a force that enters the momentum equations as a source term. Here, we consider two alternatives to model the surface tension force.

In the first model, the singular surface tension force is smoothed out over a finite thickness according to the continuum surface force model by Brackbill et al. [6]. The following force, referred to as the regularized surface tension force, is added to the Navier–Stokes equations:

$$F = \frac{1}{We} \kappa \nabla \Phi. \quad (9)$$

Here, $\mathbf{n} \delta_\Gamma$ is approximated by the gradient of the regularized indicator function Φ .

In the second model, the singular surface tension force is expressed as a line integral along the interface Γ :

$$\int_{\Omega} F \cdot \mathbf{v} d\Omega = \frac{1}{We} \int_{\Gamma} \kappa \mathbf{n} \cdot \mathbf{v} d\Gamma, \quad (10)$$

where \mathbf{v} is a finite element test function. We will refer to this as the sharp surface tension model.

Before we compute the curvature κ , which is needed for the surface tension force, we apply an intermediate projection step for $\boldsymbol{\psi}^{n+1} = (\nabla \Phi)^{n+1}$, i.e.

$$\int_{\Omega} \mathbf{v} \cdot \boldsymbol{\psi}^{n+1} + \eta_{\mathbf{n}} \nabla \mathbf{v} \cdot \nabla \boldsymbol{\psi}^{n+1} d\Omega = \int_{\Omega} \mathbf{v} \cdot \nabla \Phi^{n+1} d\Omega. \quad (11)$$

Here, \mathbf{v} denotes a piecewise vector-valued test function and $\eta_{\mathbf{n}} \geq 0$ is a filter parameter. The filter parameter is introduced to damp high frequency errors that

are magnified by differentiation and may lead to an inaccurate approximation. The projection step allows for approximating $\boldsymbol{\psi}^{n+1}$ with higher order elements than $\nabla\Phi^{n+1}$.

In level set methods, it is common to define the curvature as the divergence of the normal:

$$\kappa = \nabla \cdot \mathbf{n}. \quad (12)$$

Using approximation (11) to compute the normal, we evaluate the curvature from

$$\int_{\Omega} v \kappa^{n+1} + \eta_{\kappa} \nabla v \cdot \nabla \kappa^{n+1} d\Omega = - \int_{\Omega} \nabla v \cdot \frac{\boldsymbol{\psi}^{n+1}}{|\boldsymbol{\psi}^{n+1}|} d\Omega, \quad (13)$$

where v is a finite element test function. A filtered curvature is computed using the filter parameter $\eta_{\kappa} > 0$. The idea of filtering was also used in the volume of fluid method presented in [15]; in that context a convolution technique was used.

3.2 A coupled flow solver

The coupled method is implemented in C++ using the finite element library deal.II [23], basing the discretization on a subdivision of the domain Ω into quadrilaterals/hexahedra. A uniform mesh with mesh size h in both x - and y -directions is used. The space discretization for the method is based on the Taylor–Hood element pair $\mathcal{Q}_2\mathcal{Q}_1$ for velocity and pressure, which is LBB-stable [24]. The time discretization is performed by using a fully implicit BDF-2 time stepping scheme on the coupled velocity–pressure system.

We define a momentum residual vector for time step $n + 1$ by

$$\begin{aligned} R_i^m(\mathbf{u}^{n+1}, p^{n+1}; \mathbf{F}^{n+1}) &= \frac{1}{\Delta t} \int_{\Omega} \mathbf{v}_i \cdot \left(\frac{3}{2} \mathbf{u}^{n+1} - 2\mathbf{u}^n + \frac{1}{2} \mathbf{u}^{n-1} \right) d\Omega \\ &\quad - \int_{\Omega} \nabla \mathbf{v}_i \cdot \mathbf{u}^{n+1} d\Omega - \int_{\Omega} (\nabla \cdot \mathbf{v}_i) p^{n+1} d\Omega \\ &\quad + \frac{1}{\text{Re}} \int_{\Omega} \nabla \mathbf{v}_i \cdot \nabla^s \mathbf{u}^{n+1} d\Omega - \int_{\Omega} \mathbf{v}_i \cdot \left(\frac{1}{\text{Fr}^2} \mathbf{e}_g + \frac{1}{\text{We}} \mathbf{F}^{n+1} \right) d\Omega, \end{aligned}$$

with component i associated with the i th test function \mathbf{v}_i . Similarly, a continuity residual vector is defined by

$$R_i^c(\mathbf{u}^{n+1}, p^{n+1}; \mathbf{F}^{n+1}) = \int_{\Omega} q_i (\nabla \cdot \mathbf{u}^{n+1}) d\Omega.$$

The coupled scheme starts time step $n + 1$ with initial guesses $\mathbf{u}_0^{n+1}, p_0^{n+1}, \Phi_0^{n+1}$ that are obtained from the previous two time levels by extrapolation. In each step k ($k \geq 1$) of the nonlinear iteration, we first calculate Φ_k by solving the advection equation (6), using the old velocity \mathbf{u}_{k-1}^{n+1} , and BDF-2 time stepping. The linear equation system is solved with GMRES using an SSOR preconditioner. Then, we perform the reinitialization with the artificial time step $\Delta\tau$ in the reinitialization

equation (7) chosen to be $\Delta\tau = 0.3 \min(h, \Delta t)$. Normals and curvature κ_k^{n+1} are computed from equation (11) and (13), by using a CG solver with SSOR preconditioning, with the filter parameters $\eta_{\mathbf{n}} = 0.05h$ and $\eta_{\kappa} = h^2$, respectively. The tolerance for all the linear solvers is set to 10^{-10} . The surface tension force \mathbf{F}_k^{n+1} is computed using the regularized model, equation (9). Then, we calculate new values for velocity and pressure by solving a Newton system on the velocity/pressure system, i.e., we solve for

$$\mathbf{J}(\mathbf{u}_{k-1}^{n+1}) \begin{pmatrix} \Delta \mathbf{U}_k \\ \Delta \mathbf{P}_k \end{pmatrix} = - \begin{pmatrix} \mathbf{R}^m(\mathbf{u}_{k-1}^{n+1}, p_{k-1}^{n+1}, \mathbf{F}_k^{n+1}) \\ \mathbf{R}^c(\mathbf{u}_{k-1}^{n+1}, p_{k-1}^{n+1}, \mathbf{F}_k^{n+1}) \end{pmatrix},$$

and then set update velocity and pressure by

$$\begin{pmatrix} \mathbf{U}_k^{n+1} \\ \mathbf{P}_k^{n+1} \end{pmatrix} = \begin{pmatrix} \mathbf{U}_{k-1}^{n+1} \\ \mathbf{P}_{k-1}^{n+1} \end{pmatrix} + \begin{pmatrix} \Delta \mathbf{U}_k \\ \Delta \mathbf{P}_k \end{pmatrix}.$$

The vectors \mathbf{U}_k^{n+1} and \mathbf{P}_k^{n+1} denote the discrete values of \mathbf{u}_k^{n+1} and p_k^{n+1} at the finite element interpolation points, and $\mathbf{J}(\mathbf{u}_{k-1}^{n+1})$ denotes the (consistent) Jacobian matrix related to the residual \mathbf{R} , evaluated at the old iterate. The discrete system is solved with BiCGStab using a Schur complement preconditioner [25] to a tolerance 10^{-10} . The nonlinear system is iterated until the residual \mathbf{R} is smaller than 10^{-10} , measured in the discrete l_2 norm.

This procedure combines a Newton iteration for the Navier–Stokes system with the advection equation (6) and surface tension force evaluation in (9) in a Gauss–Seidel-like iteration scheme. We obtain a fully-coupled scheme for velocities, pressure, and the level set function Φ at time level $n + 1$. We emphasize that this fully coupled system has been used with the purpose to display an algebraically balanced scheme. A more practically relevant implementation of a coupled scheme would avoid the outer coupling of the Navier–Stokes system with the level set equation through the Gauss–Seidel iteration, and just use a coupled Navier–Stokes system.

3.3 A decoupled flow solver

The numerical simulations with the decoupled solver are implemented using FemLego, a parallel finite element code for solving partial differential equations [26]. We use uniform meshes of triangles with mesh size h in both x - and y -directions.

The Navier–Stokes equations are discretized using a fractional step projection method [27]. At each time step an intermediate velocity, denoted by \mathbf{u}_*^{n+1} , is computed

$$\begin{aligned} \frac{1}{\Delta t} \int_{\Omega} (\mathbf{u}_*^{n+1} - \mathbf{u}^n) \cdot \mathbf{v} d\Omega - \int_{\Omega} (\mathbf{u}_*^n \cdot \nabla \mathbf{v}) \cdot \mathbf{u}_*^{n+1} d\Omega = - \int_{\Omega} \mathbf{v} \cdot \nabla p^n d\Omega - \\ \frac{1}{\text{Re}} \int_{\Omega} \sum_j \nabla \mathbf{v}_j \cdot (\nabla \mathbf{u}_{*j}^{n+1} + \mathbf{u}_{x_j}^n) d\Omega + \int_{\Omega} \mathbf{v} \cdot \left(\frac{1}{\text{Fr}^2} \mathbf{e}_g + \frac{1}{\text{We}} \mathbf{F}^n \right) d\Omega, \end{aligned} \quad (14)$$

where \mathbf{F}^n is the surface tension force. The above equation is to hold for all test functions \mathbf{v} that are in the approximate solution space. We use either piecewise quadratic elements \mathcal{P}_2 or piecewise linear elements \mathcal{P}_1 . The intermediate velocity field is not necessarily divergence free. By requiring the final velocity field to be solenoidal, one obtains a Poisson equation for the pressure p^{n+1} ,

$$\frac{-1}{\Delta t} \int_{\Omega} q \nabla \cdot \mathbf{u}_*^{n+1} d\Omega = \int_{\Omega} \nabla q \cdot \nabla (p^{n+1} - p^n) d\Omega - \varepsilon_p \frac{h^2}{\Delta t} \int_{\Omega} \nabla q \cdot \nabla p^{n+1} d\Omega,$$

where the test function q belongs to the space of piecewise linear functions. The stabilization parameter $\varepsilon_p \neq 0$ is needed when the element pair (\mathbf{v}, q) that is used for velocity and pressure approximation does not satisfy the LBB condition, see, e.g., [24]. We refer to this approach of stabilizing the finite element discretization as the naive approach. Stabilization is needed for the element pair $\mathcal{P}_1 \mathcal{P}_1$ while the Taylor–Hood element pair $\mathcal{P}_2 \mathcal{P}_1$ is LBB-stable and $\varepsilon_p = 0$.

The pressure p^{n+1} is used to update the velocity

$$\int_{\Omega} \mathbf{v} \cdot \frac{\mathbf{u}^{n+1} - \mathbf{u}_*^{n+1}}{\Delta t} d\Omega = - \int_{\Omega} \mathbf{v} \cdot \nabla (p^{n+1} - p^n) d\Omega + \varepsilon_p \frac{h^2}{\Delta t} \int_{\Omega} \mathbf{v} \cdot \nabla p^{n+1} d\Omega.$$

All the discretized equations are solved using GMRES or the conjugate gradient method with tolerance 10^{-10} . Unless stated otherwise, normals and curvature are computed from equation (11) and (13), with the filter parameters $\eta_{\mathbf{n}} = \eta_{\kappa} = 0$.

4 Factors affecting spurious currents

Consider a circular drop in equilibrium in the interior of the domain and neglect gravitational effects. Since the velocity is zero, the Navier–Stokes equations (1) reduce to

$$\nabla p = \frac{1}{\text{We}} \kappa \mathbf{n} \delta(\Gamma) = \frac{1}{\text{We}} \kappa \nabla I_{\Gamma}, \quad (15)$$

where I_{Γ} is the indicator function that changes from 1 to 0 at the interface Γ . For a two dimensional circular drop the exact curvature is $\kappa_{\text{exact}} = 1/R$, and the pressure is given by

$$p_{\text{exact}} = \frac{1}{R \text{We}} I_{\Gamma}. \quad (16)$$

Since the exact solution for the velocity is zero, we will regard non-zero velocities in the system as spurious currents. In the following sections, we will investigate how spurious currents depend on the capillary number, the spatial mesh size, the time step, the interface thickness, the representation of the surface tension force, the finite element spaces used, and the curvature evaluation. While investigating a certain factor, we try to eliminate effects from the other factors. We also study the influence of the fractional step projection method by comparing the coupled and the decoupled method described in Sections 3.2 and 3.3, respectively. Unless stated otherwise, we use $\mathcal{Q}_2 \mathcal{Q}_1 \mathcal{Q}_1$ elements for velocity, pressure,

and Φ in the coupled method. In the decoupled method we use $\mathcal{P}_2\mathcal{P}_1\mathcal{P}_1$ elements. Except in one set of computations, we use the regularized surface tension force defined in equation (9) with the curvature computed as in equation (13). Besides the spurious currents, we also measure how accurate the method predicts the difference in pressure between the inside and the outside of the bubble.

The computational domain in non-dimensional coordinates is $\{(x, y) : -2.5 \leq x \leq 2.5, 0 \leq y \leq 5\}$. The drop is centered at $(x_c, y_c) = (0, 2.5)$ and has non-dimensional radius $R = 0.5$. For the numerical calculation, we measure the pressure p_{inner} inside the drop as the average of the pressure on a circle of diameter 0.2 centered at (x_c, y_c) . The outside pressure p_{outer} is measured as the average of the pressure along the boundary of the domain, $\partial\Omega$. The relative error in pressure is then defined as

$$\Delta p_{\text{rel}} = \frac{|p_{\text{exact}} - (p_{\text{inner}} - p_{\text{outer}})|}{p_{\text{exact}}}. \quad (17)$$

We assume a Reynolds number $\text{Re} = 10$ and employ capillary numbers Ca between 10^{-3} and 1. The level set function is initialized as the regularized indicator function in equation (5) with $d(x, y) = \sqrt{x^2 + (y - y_c)^2} - R$.

4.1 Capillary number

We vary the capillary number between 1 and 0.001 in order to investigate how spurious currents and errors in pressure depend on the capillary number. We use a uniform mesh with $h = 0.0148$ and set the interface thickness to $\varepsilon = 3h$. With this choice of ε , the level set function is well resolved. The interval around the interface where Φ varies between 0.05 and 0.95 is 18 cells wide. In Table 1 we report the magnitude of spurious currents for the different capillary numbers using both the coupled and the decoupled method. We see that both the (absolute) error in the pressure jump and the spurious currents are proportional to $1/\text{Ca}$, in agreement with [12]. The result is similar for the coupled and the decoupled method.

Figs. 2 and 3 show how the magnitude of spurious currents changes with time. We see that the spurious currents first increase and then reach a steady value. The magnitude of the spurious currents reported in Table 1 is the maximum value obtained over time. Fig. 4 shows the spurious currents at two time instants for $\text{Ca} = 0.1$ using the coupled method. The first figure illustrates the velocity field at time $t = 0.28$ when the maximum velocity is obtained. Eight vortices around the interface can be observed. The second figure shows the flow field when the magnitude of spurious currents has leveled off. Then, the vortices are smaller and alternate direction with a period of about 1.2 time units. Comparing the two pictures one can observe that the spurious currents extend over a larger domain at the later time, but the magnitude of velocity is smaller.

Table 1: Maximum magnitude of the spurious currents over time for different capillary numbers Ca using $h = 0.0148$ and $\varepsilon = 3h$.

Ca	coupled method			decoupled method		
	Δt	$\ \mathbf{u}\ _{\infty}^{\text{coup}}$	$\Delta p_{\text{rel}}^{\text{coup}}$	Δt	$\ \mathbf{u}\ _{\infty}^{\text{decoup}}$	$\Delta p_{\text{rel}}^{\text{decoup}}$
0.001	$5 \cdot 10^{-5}$	$2.7 \cdot 10^{-3}$	3.2%	10^{-6}	$5.4 \cdot 10^{-3}$	2.9%
0.01	$5 \cdot 10^{-4}$	$7.4 \cdot 10^{-4}$	3.2%	10^{-5}	$1.0 \cdot 10^{-3}$	2.9%
0.1	$5 \cdot 10^{-3}$	$1.2 \cdot 10^{-4}$	3.2%	10^{-4}	$1.7 \cdot 10^{-4}$	2.9%
1	$5 \cdot 10^{-2}$	$1.4 \cdot 10^{-5}$	3.2%	10^{-3}	$3.4 \cdot 10^{-5}$	2.9%

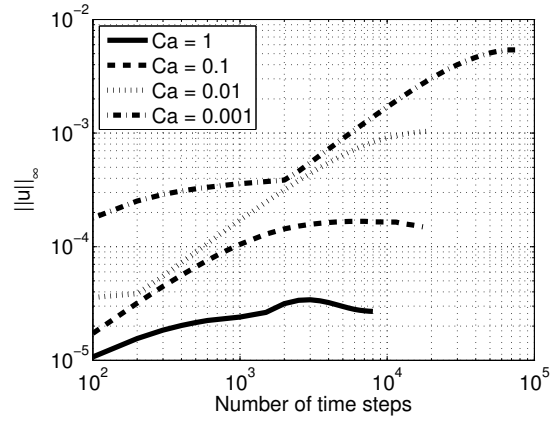


Figure 2: $\|\mathbf{u}\|_{\infty}^{\text{decoup}}$ as a function of number of time steps for different capillary numbers using $h = 0.0148$, $\varepsilon = 3h$, and Δt according to Table 1.

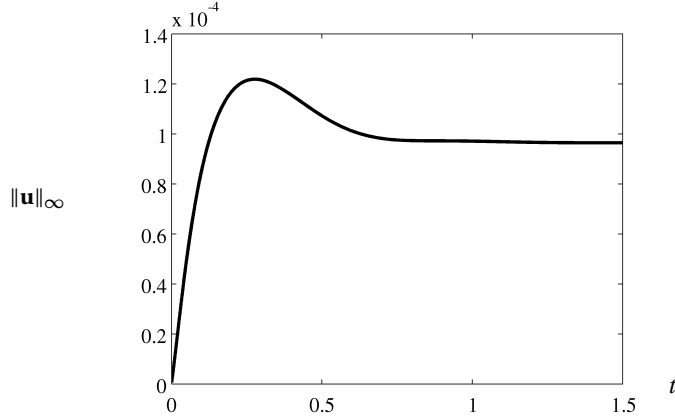


Figure 3: $\|\mathbf{u}\|_{\infty}^{\text{coup}}$ as a function of time for $\text{Ca} = 0.1$ using $h = 0.0148$, $\varepsilon = 3h$, and $\Delta t = 5 \cdot 10^{-3}$.

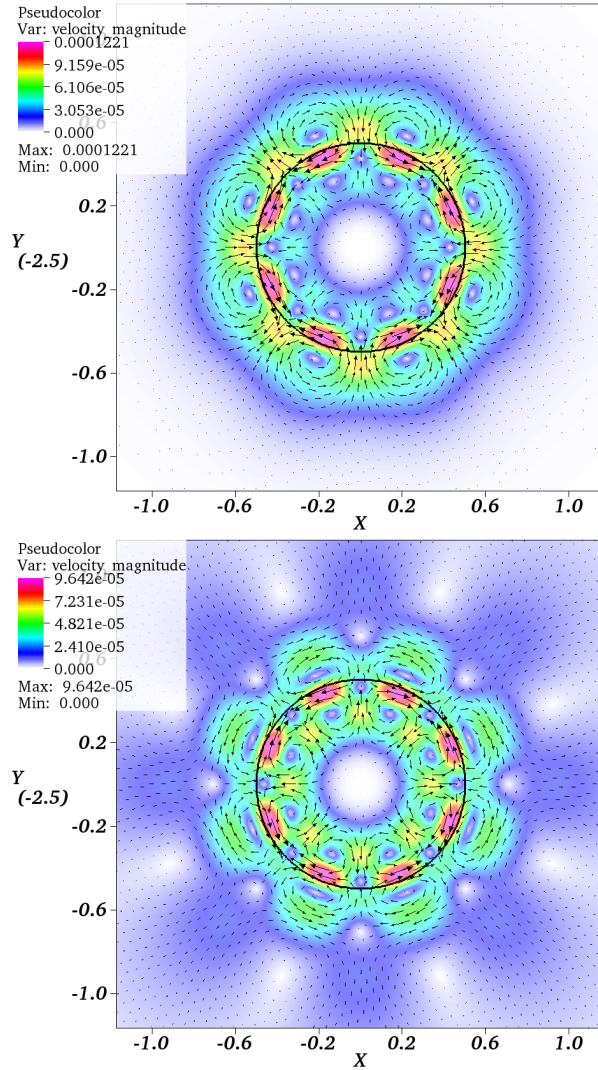


Figure 4: Direction and magnitude of spurious currents around the interface (indicated by the black line) at time $t = 0.2$ (upper) and $t = 2$ (lower). The coupled method is used, $Ca = 0.1$, $h = 0.0148$, and $\Delta t = 5 \cdot 10^{-3}$.

4.2 Spatial mesh size

In the sequel, we focus on the case $Ca = 0.1$. We investigate spurious currents and the error in pressure for different mesh sizes with the interface thickness $\varepsilon = 3h$. The maximum magnitude of the spurious currents as well as the relative error in pressure for different mesh sizes are presented in Table 2. As we reduce the mesh size, the interface representation becomes sharper, the pressure representation improves, and the spurious currents are reduced. We observe a quadratic

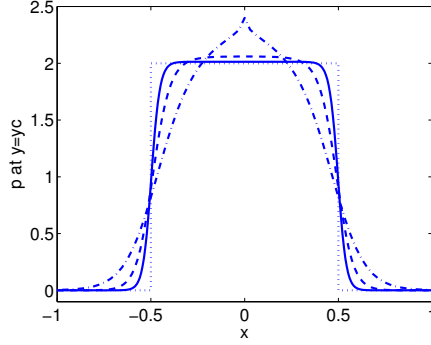


Figure 5: Cross sections of the pressure through $y = 2.5$ for three different mesh sizes. The capillary number $Ca = 0.1$, the step size $\Delta t = 1 \cdot 10^{-4}$ and $\varepsilon = 3h$. Dotted line: The exact pressure. Solid line: $h = 7.40 \cdot 10^{-3}$. Dashed line: $h = 1.48 \cdot 10^{-2}$. Dash dotted line: $h = 2.96 \cdot 10^{-2}$.

convergence rate for the pressure in both the coupled and the decoupled methods. The convergence rate for the velocity measured in the L_∞ -norm is between linear and quadratic in both methods. The spurious currents extend over larger domains for larger mesh sizes. The convergence rate measured in the L_2 -norm is similar. We have also performed computations for other values of Ca and ε and obtained convergence.

Table 2: The maximum magnitude of the spurious currents over time for different mesh sizes h and $\varepsilon = 3h$. The result indicate second order and superlinear convergence for the pressure jump and the velocity, respectively.

h	coupled method			decoupled method		
	Δt	$\ \mathbf{u}\ _\infty^{\text{coup}}$	$\Delta p_{\text{rel}}^{\text{coup}}$	Δt	$\ \mathbf{u}\ _\infty^{\text{decoup}}$	$\Delta p_{\text{rel}}^{\text{decoup}}$
$2.96 \cdot 10^{-2}$	$5 \cdot 10^{-3}$	$4.4 \cdot 10^{-4}$	14%	$2 \cdot 10^{-4}$	$7.4 \cdot 10^{-4}$	9.6%
$1.48 \cdot 10^{-2}$	$5 \cdot 10^{-3}$	$1.2 \cdot 10^{-4}$	3.2%	$1 \cdot 10^{-4}$	$1.7 \cdot 10^{-4}$	2.9%
$7.40 \cdot 10^{-3}$	$5 \cdot 10^{-3}$	$3.1 \cdot 10^{-5}$	0.71%	$5 \cdot 10^{-5}$	$5.1 \cdot 10^{-5}$	0.67%

4.3 Time step

We investigate here how spurious currents depend on the time step. We focus on the case when $Ca = 0.1$ and $h = 1.48 \cdot 10^{-2}$. Table 3 shows that the results converge to non-zero values as the time step is reduced. The errors are dominated by the spatial discretization as soon as $\Delta t \leq 2 \cdot 10^{-4}$ for the decoupled method and $\Delta t \leq 2 \cdot 10^{-2}$ for the coupled method. This indicates that we can take larger time steps in the coupled method without losing accuracy.

Table 3: The magnitude of the spurious currents at $t = 0.3$ for different time steps Δt . The mesh size $h = 1.48 \cdot 10^{-2}$ and $\varepsilon = 3h$.

coupled method			decoupled method		
Δt	$\ \mathbf{u}\ _{\infty}^{\text{coup}}$	$\Delta p_{\text{rel}}^{\text{coup}}$	Δt	$\ \mathbf{u}\ _{\infty}^{\text{decoup}}$	$\Delta p_{\text{rel}}^{\text{decoup}}$
$4 \cdot 10^{-2}$	$1.0 \cdot 10^{-4}$	3.2%	$4 \cdot 10^{-4}$	$1.3 \cdot 10^{-4}$	2.9%
$2 \cdot 10^{-2}$	$1.2 \cdot 10^{-4}$	3.2%	$2 \cdot 10^{-4}$	$1.6 \cdot 10^{-4}$	2.9%
$5 \cdot 10^{-5}$	$1.2 \cdot 10^{-4}$	3.2%	$5 \cdot 10^{-5}$	$1.6 \cdot 10^{-4}$	2.9%

4.4 Interface thickness

The interface thickness is controlled by the parameter ε in the reinitialization scheme (7). As ε decreases the level set function becomes sharper and closer to an indicator function. We have made computations with decreasing ε , keeping the mesh size, the time step, and the capillary number fixed. The coupled and the decoupled method behave in a similar way, therefore we report results from only one of the methods.

In Fig. 6 we see that decreasing ε leads to better pressure representation. However, Table 4 shows that the spurious currents increase somewhat when the thickness of the interface ε becomes large or small relative to the mesh size. This is because the computation of normals, curvature and surface tension force is not accurate in those cases.

Table 4: The maximum magnitude of the spurious currents over time for different values of ε . We use $h = 0.0148$ and $\Delta t = 5 \cdot 10^{-3}$.

ε	$\ \mathbf{u}\ _{\infty}^{\text{coup}}$	$\Delta p_{\text{rel}}^{\text{coup}}$
$4h$	$1.3 \cdot 10^{-4}$	5.9%
$2h$	$1.0 \cdot 10^{-4}$	1.4%
h	$1.1 \cdot 10^{-4}$	0.50%
$h/2$	$1.4 \cdot 10^{-4}$	0.37%

4.5 Representation of the surface tension force

In this section we use the exact curvature $\kappa = \frac{1}{R} = 2$ to separate effects of how surface tension is modeled, from effects of errors in the approximation of the curvature. We use the decoupled method and consider both the regularized surface tension force defined in equation (9) and the sharp surface tension force defined in equation (10). In Table 5 we see that when the regularized surface tension force is used, spurious currents are of the order of tolerance of the lin-

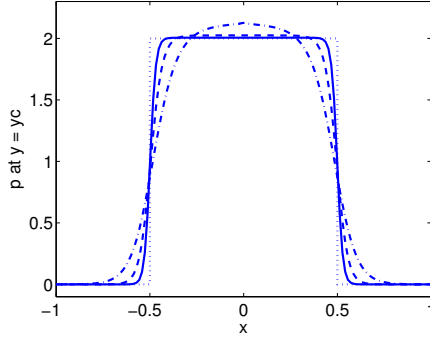
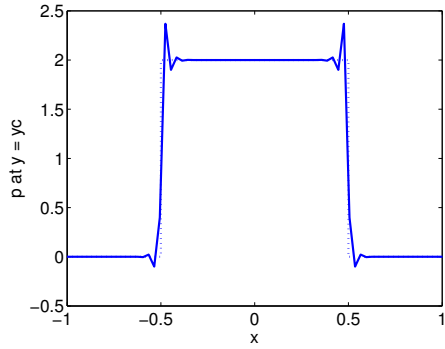


Figure 6: Cross sections of the pressure through $y = 2.5$ is shown for $\varepsilon = 4h, 2h, h$. Dotted line: The exact pressure. Solid line: $\varepsilon = h$. Dashed line: $\varepsilon = 2h$. Dash dotted line: $\varepsilon = 4h$. We use $h = 1.48 \cdot 10^{-2}$ and $\Delta t = 1 \cdot 10^{-4}$.

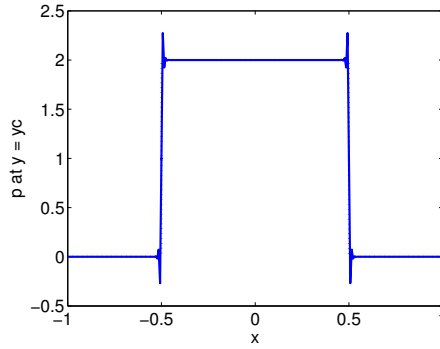
ear solver. The error in the pressure jump decreases exponentially with mesh refinement. This indicates that the pressure gradient and the regularized surface tension force are in balance with the chosen discretization. However, when the sharp surface tension force is used, we observe very large spurious currents close to the interface. Although the spurious currents and the jump in the pressure converge as the mesh is refined, we can see in Fig. 7 that the oscillations in pressure close to the interface do not decrease as the spatial mesh size is reduced. The reason for this is that we try to approximate a discontinuous function with continuous piecewise polynomials. For the sharp surface tension force to be in balance with the pressure gradient, one would need to be able to represent the pressure as a discontinuous function. The work by Ganesan et al. [18] shows that with a continuous representation of the pressure, spurious currents are present even when isoparametric finite elements are used.

Table 5: The magnitude of the spurious currents at steady state. The *exact curvature* $\kappa = 2$ is prescribed.

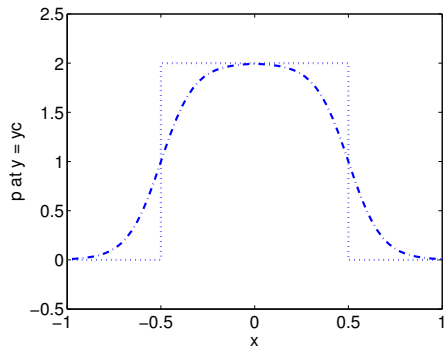
h	Δt	Regularized force		Sharp force	
		$\ \mathbf{u}\ _{\infty}^{\text{decoup}}$	$\Delta p_{\text{rel}}^{\text{decoup}}$	$\ \mathbf{u}\ _{\infty}^{\text{decoup}}$	$\Delta p_{\text{rel}}^{\text{decoup}}$
$2.96 \cdot 10^{-2}$	$2 \cdot 10^{-4}$	$\mathcal{O}(10^{-11})$	1.1%	$3.5 \cdot 10^{-2}$	$2 \cdot 10^{-4}\%$
$1.48 \cdot 10^{-2}$	$1 \cdot 10^{-4}$	$\mathcal{O}(10^{-11})$	$1.3 \cdot 10^{-2}\%$	$2.0 \cdot 10^{-2}$	$1.4 \cdot 10^{-6}\%$
$7.40 \cdot 10^{-3}$	$5 \cdot 10^{-5}$	$\mathcal{O}(10^{-11})$	$6.1 \cdot 10^{-8}\%$	$1.1 \cdot 10^{-2}$	$4.8 \cdot 10^{-8}\%$



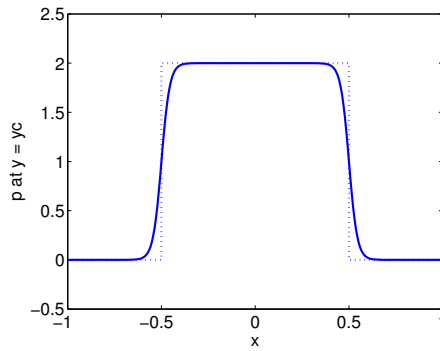
(a) Sharp interface force. Coarse mesh.



(b) Sharp interface force. Fine mesh.



(c) Regularized interface force. Coarse mesh.



(d) Regularized interface force. Fine mesh.

Figure 7: Cross section of the pressure through $y = 2.5$. The exact curvature $\kappa = 2$ is prescribed and $\varepsilon = 3h$. The dotted line is the exact pressure given in equation (16). Panels (a) and (c): $h = 2.96 \cdot 10^{-2}$ and $\Delta t = 2 \cdot 10^{-4}$. Panels (b) and (d): $h = 7.40 \cdot 10^{-3}$ and $\Delta t = 5 \cdot 10^{-5}$.

4.6 Finite element spaces

Throughout this section, we use the exact curvature $\kappa = \frac{1}{R} = 2$ and the regularized surface tension force and investigate the effect of using different finite element combinations.

From Table 6 and 7 we see that spurious currents are present when the pressure and the regularized indicator function Φ^ε are approximated in different finite element spaces. When the same finite elements are used to approximate the pressure and the regularized indicator function Φ^ε spurious currents are of the order of the tolerance of the linear solvers. Thus,

$$\nabla_h p_h = \frac{1}{RWe} \nabla_h \Phi_h^\varepsilon, \quad (18)$$

and exact force balance is possible both for the coupled method as well as for the decoupled method.

Further investigations using the element triple $(\mathbf{u}, p, \Phi) = \mathcal{P}_2 \mathcal{P}_1 \mathcal{P}_2$ show that the magnitude of spurious currents increases rapidly as the regularization parameter decreases, see Table 8. However, for a fixed ε we observe fourth order convergence for the spurious currents as the mesh is refined, see Table 9.

When equal-order elements are used to approximate pressure and velocity, the LBB-condition is not satisfied and stabilization is necessary in order to guarantee a unique solution. A naive approach is to change the incompressibility condition to $\nabla \cdot \mathbf{u} - \varepsilon_p h^2 \nabla^2 p = 0$. We see from Table 7 that the size of spurious currents depends on the size of the stabilization term ε_p . Thus, the force balance is destroyed. However, from Table 6 we see that the spurious currents are again of the order of the tolerance of the linear solver when the streamline-upwind/Petrov-Galerkin (SUPG) and pressure-stabilizing/Petrov-Galerkin (PSPG) formulations are used for stabilization [24].

With the same finite elements used to approximate the pressure and the regularized indicator function, the discrete pressure $p_h = \Phi_h^\varepsilon / (RWe)$. Thus, the error in pressure depends solely on the regularization parameter ε . When the regularization parameter is fixed, the relative error in the pressure jump does not decrease with mesh refinement, see Table 9. In fact, the relative error in the pressure jump is exactly equal to the difference between the regularized indicator function of equation (5) and the exact indicator function evaluated in analogy with equation (17). Therefore, in the calculations presented in Table 10, where the regularization parameter ε is proportional to the mesh size, the relative error in pressure decreases exponentially. The error in the pressure jump decreases more slowly (but still exponentially) when different element spaces are used for pressure and regularized indicator function, compare with Table 5.

In the volume-of-fluid method presented in [13], a key idea was to use the same finite difference method for discretizing ∇p as for $\nabla \Phi$ to obtain balance between the forces. In the volume-of-fluid method, the function Φ represents the volume fraction of one of the fluids in each cell.

Even if equal order elements are used to approximate the pressure and the regularized indicator function, the forces may be unbalanced due to errors in the computation of the curvature. This source of errors is studied in the next section.

Table 6: The magnitude of the spurious currents and the relative error in pressure for $h = 0.0148$, $\varepsilon = 3h$, and $\Delta t = 5 \cdot 10^{-3}$ at steady state. The *exact curvature* $\kappa = 2$ prescribed. The coupled method is used.

Element (\mathbf{u}, p, Φ)	Stabilization	$\ \mathbf{u}\ _\infty$	Δp_{rel}
$\mathcal{Q}_2\mathcal{Q}_1\mathcal{Q}_1$	none	$\mathcal{O}(10^{-14})$	0.0065%
$\mathcal{Q}_2\mathcal{Q}_1\mathcal{Q}_2$	none	$4.7 \cdot 10^{-6}$	0.0068%
$\mathcal{Q}_1\mathcal{Q}_1\mathcal{Q}_1$	$\varepsilon_p = 1$	$7.2 \cdot 10^{-4}$	0.0071%
$\mathcal{Q}_1\mathcal{Q}_1\mathcal{Q}_1$	SUPG/PSPG	$\mathcal{O}(10^{-13})$	0.0066%

Table 7: The magnitude of the spurious currents and the relative error in pressure for $h = 0.0148$, $\varepsilon = 3h$, and $\Delta t = 10^{-4}$ at steady state. The *exact curvature* $\kappa = 2$ is prescribed. The decoupled method is used.

Element (\mathbf{u}, p, Φ)	Stabilization	$\ \mathbf{u}\ _\infty$	Δp_{rel}
$\mathcal{P}_2\mathcal{P}_1\mathcal{P}_1$	none	$\mathcal{O}(10^{-12})$	0.013%
$\mathcal{P}_2\mathcal{P}_1\mathcal{P}_2$	none	$8.2 \cdot 10^{-6}$	0.013%
$\mathcal{P}_1\mathcal{P}_1\mathcal{P}_1$	$\varepsilon_p = 10^{-4}$	$5.0 \cdot 10^{-7}$	0.013%
$\mathcal{P}_1\mathcal{P}_1\mathcal{P}_1$	$\varepsilon_p = 10^{-2}$	$5.0 \cdot 10^{-5}$	0.013%

Table 8: The magnitude of the spurious currents and the relative error in pressure for $\text{Ca} = 0.1$, $h = 1.48 \cdot 10^{-2}$, and $\Delta t = 1 \cdot 10^{-4}$. The *exact curvature* $\kappa = 2$ is prescribed. The decoupled method is used. The element triple (\mathbf{u}, p, Φ) = $\mathcal{P}_2\mathcal{P}_1\mathcal{P}_2$ is used.

ε	$\ \mathbf{u}\ _\infty$	Δp_{rel}
$3h$	$8.2 \cdot 10^{-6}$	$1.3 \cdot 10^{-2}\%$
$2.5h$	$1.4 \cdot 10^{-5}$	$2.0 \cdot 10^{-3}\%$
h	$2.4 \cdot 10^{-4}$	$8.7 \cdot 10^{-7}\%$

4.7 Curvature evaluation

When the surface tension force is regularized, a volume force has to be evaluated. A curvature must be defined in the domain where the regularized surface tension force has its support. In this section, we study two different ways to define curvature away from the interface.

One way is to use the curvature of the level set of Φ . Numerically, this curvature can be computed as the divergence of the normal as in equation (12). In the case

Table 9: The magnitude of the spurious currents and the relative error in pressure for $Ca = 0.1$ and $\varepsilon = 0.0444$. The *exact curvature* $\kappa = 2$ is prescribed. The decoupled method is used. The element triple $(\mathbf{u}, p, \Phi) = \mathcal{P}_2\mathcal{P}_1\mathcal{P}_2$ is used. We observe a fourth order convergence for the velocity when the mesh is refined. The error in pressure has almost converged.

h	Δt	$\ \mathbf{u}\ _\infty$	Δp_{rel}
$1.48 \cdot 10^{-2}$	$1 \cdot 10^{-4}$	$8.2 \cdot 10^{-6}$	$1.3 \cdot 10^{-2}\%$
$1.05 \cdot 10^{-2}$	$7 \cdot 10^{-5}$	$2.0 \cdot 10^{-6}$	$1.3 \cdot 10^{-2}\%$
$7.40 \cdot 10^{-3}$	$5 \cdot 10^{-5}$	$5.0 \cdot 10^{-7}$	$1.2 \cdot 10^{-2}\%$

Table 10: The magnitude of the spurious currents and the relative error in pressure for $Ca = 0.1$ and $\varepsilon = 3h$. The *exact curvature* $\kappa = 2$ is prescribed. The decoupled method is used. The element triple $(\mathbf{u}, p, \Phi) = \mathcal{P}_2\mathcal{P}_1\mathcal{P}_2$ is used. We observe a first order convergence for the velocity as the mesh and ε decreases. The error in pressure decreases exponentially as ε and the mesh size decreases.

h	Δt	$\ \mathbf{u}\ _\infty$	Δp_{rel}
$2.96 \cdot 10^{-2}$	$2 \cdot 10^{-4}$	$1.7 \cdot 10^{-5}$	1.2%
$1.48 \cdot 10^{-2}$	$1 \cdot 10^{-4}$	$8.2 \cdot 10^{-6}$	$1.3 \cdot 10^{-2}\%$
$7.40 \cdot 10^{-3}$	$5 \cdot 10^{-5}$	$4.0 \cdot 10^{-6}$	$1.4 \cdot 10^{-5}\%$

of a circular drop centered at $(0, y_c)$, the analytical curvature of the level set at a point (x, y) is given by

$$\kappa = \frac{1}{\sqrt{x^2 + (y - y_c)^2}}. \quad (19)$$

Another way is to use the curvature at the closest point on the interface. In the case of a static circular drop with radius $R = 0.5$, the analytical curvature at any point on the interface is given by $\kappa = \frac{1}{R} = 2$. Numerically, the nearest point on the interface for a given node point in two dimensions can be found using the method developed by Chopp [28]. We use a formula given in [29] which gives a good approximation when the interface is close to a circle:

$$\kappa = \frac{1}{1/(\nabla \cdot \mathbf{n}) - d(\Phi)}. \quad (20)$$

The signed distance function d is computed from the regularized indicator function Φ assuming it has the form given by equation (5).

The results presented in Table 11 are with $h = 0.0148$ and $\varepsilon = 2.5h$. The magnitudes of the spurious currents are much larger when the curvature is computed numerically (rows 2 and 4 in Table 11) compared to when the analytical expressions are used (rows 1 and 3). We also see that with the analytical expressions for the curvature, spurious currents are smaller when we use the curvature at the interface (row 1), rather than the curvature of the level set (row 3).

In order to understand the difference in pressure between the different curvature extensions we rewrite equation (15) in polar coordinates (r, θ) with I_Γ replaced by Φ^ε (defined as in equation (5)). The pressure in polar coordinates is given by

$$p(r) = \frac{1}{\text{We}} \int_{r_0}^r \kappa(s) \frac{\partial \Phi^\varepsilon}{\partial s} ds. \quad (21)$$

Here we let $r_0 = 2.5$ which corresponds to the boundary of our computational domain and we assume $p(r_0) = 0$. Computing the relative error for the pressure jump by evaluating the pressure as in equation (21) we get for $\varepsilon = 0.037$ a relative error $\Delta p_{\text{rel}} = 0.0020\%$ when $\kappa(r) = 2$ and $\Delta p_{\text{rel}} = 2.0\%$ when $\kappa(r) = 1/r$. These values are exactly the ones we get by solving the full Navier–Stokes equations, see Table 11. Note that analytically the surface tension force depends only on r . However, in a numerical implementation the force may vary slightly in the θ direction which can result in spurious currents.

In Fig. 8, a cross section of the pressure is shown for the different ways of computing the curvature. In Panel (a) we compare the analytical expressions for the curvature and in Panel (b) the numerical expressions. From Fig. 8 and Table 11 it is clear that the best results are obtained when the curvature at the interface is used. We also note that when the curvature at the level set is used, the error in pressure is the same for the analytical and the numerical expressions.

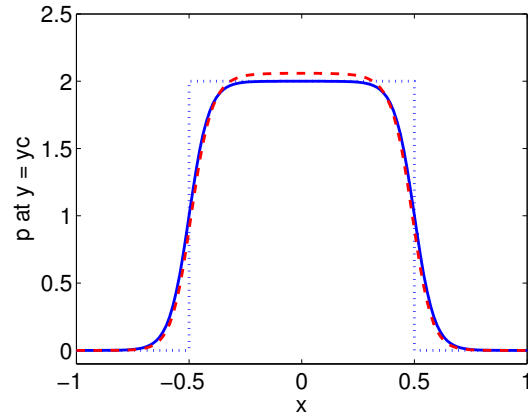
Finally, we note that as long as the level set function is reasonably well resolved (i.e. $\varepsilon > h$), the effect of using an approximate curvature dominates over the effect of using mismatching elements for the regularized indicator function and the pressure.

Table 11: The magnitude of spurious currents for different curvature calculations using $\mathcal{P}_2\mathcal{P}_1\mathcal{P}_1$ elements. The mesh size $h = 0.0145$, $\varepsilon = 2.5h$, and $\Delta t = 10^{-4}$.

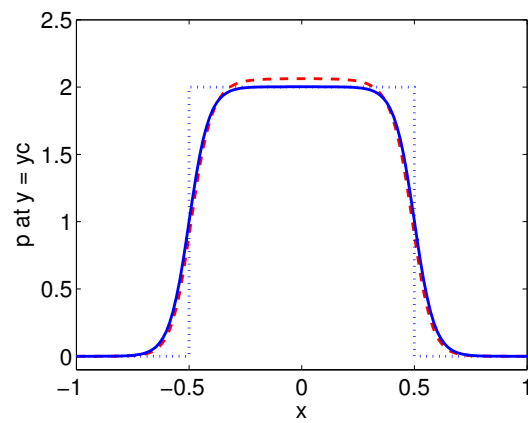
Curvature	$\ \mathbf{u}\ _\infty$	Δp_{rel}
$\kappa = 2$	$\mathcal{O}(10^{-12})$	0.0020%
$\kappa = \frac{1}{1/(\nabla \cdot \mathbf{n}) - d(\Phi)}$	$1.9 \cdot 10^{-4}$	0.12%
$\kappa = -\frac{1}{\sqrt{x^2 + (y - y_c)^2}}$	$4.4 \cdot 10^{-5}$	2.0%
$\kappa = -\nabla \cdot \mathbf{n}$	$1.8 \cdot 10^{-4}$	2.0%

4.7.1 Filtered curvature

We close this section by investigating the effect of filtering to damp high frequency errors in the numerically computed curvature. Such errors occur where the level set function is almost constant and not close to the interface. We have observed that high frequency errors in the curvature are more pronounced when higher order elements for the level set function are used.



(a) Analytic expressions for the curvature



(b) Numerically computed curvature

Figure 8: The cross section of the pressure for different curvature computations. Solid line: curvature at the closest point on the interface. Dashed line: curvature of the level sets of ϕ . Dotted line: exact pressure defined in equation (16).

A filtered curvature can be obtained either by direct filtering in the curvature computation by choosing $\eta_\kappa > 0$ in equation (13) or by computing the curvature from a filtered normal. A filtered normal $\tilde{\mathbf{n}}$ is obtained by taking $\eta_{\mathbf{n}} > 0$ in equation (11).

Table 12 shows that the spurious currents are reduced when filtering is applied. Comparing the two ways above to do the filtering, the magnitude of the spurious currents is smaller when filtering is applied directly in the curvature computation. However, filtering in the curvature has a negative impact on the pressure error. Computing the curvature from a filtered normal does not affect the pressure error. This also explains the somewhat larger error in the pressure jump in the coupled method where $\eta_\kappa = h^2$ compared to the decoupled method where $\eta_\kappa = 0$, see Table 1.

Table 12: The magnitude of spurious currents with and without damping the high frequencies in the curvature computation. The mesh size $h = 0.0145$, $\varepsilon = 2.5h$, $\Delta t = 10^{-4}$, and we use $\mathcal{P}_2\mathcal{P}_1\mathcal{P}_1$ elements.

Curvature	$\eta_{\mathbf{n}}$	η_κ	$\ \mathbf{u}\ _\infty$	Δp_{rel}
$\kappa = -\nabla \cdot \mathbf{n}$	0	0	$1.8 \cdot 10^{-4}$	2.0%
$\kappa = -\nabla \cdot \mathbf{n}$	0	h^2	$1.5 \cdot 10^{-4}$	2.1%
$\kappa = -\nabla \cdot \mathbf{n}$	0	$0.5h$	$1.1 \cdot 10^{-4}$	4.0%
$\kappa = -\nabla \cdot \tilde{\mathbf{n}}$	h^2	0	$1.7 \cdot 10^{-4}$	2.0%
$\kappa = -\nabla \cdot \tilde{\mathbf{n}}$	$0.5h$	0	$1.4 \cdot 10^{-4}$	2.0%

5 Conclusion

We have studied spurious currents appearing in two phase flow simulations using the conservative level set method and finite element discretizations. For this purpose we have considered a circular drop in equilibrium.

In all the simulations considered in this paper the magnitude of spurious currents decreases with mesh refinement. We found no significant difference between the coupled method and the decoupled method. However, larger time steps can be used in the coupled method without losing accuracy.

The most significant factor affecting the spurious currents is the representation of the surface tension. A sharp surface tension, represented as a line integral in the variational formulation, resulted in much larger errors than a regularized surface tension force. The sharp formulation also resulted in oscillations in the pressure that did not vanish with mesh refinement. This is probably related to the fact that our finite element method does not allow for discontinuities in the pressure.

Another significant factor is the combination of finite element spaces. We have found that if the same finite element space for the pressure and the regularized indicator function is used, exact force balance can be achieved, eliminating spurious currents. When an element pair for velocity and pressure is used that does not satisfy the LBB-condition, we show that a naive approach of stabilization destroys the force balance. The force balance can be retained by using the more sophisticated streamline-upwind Petrov-Galerkin and pressure-stabilizing Petrov-Galerkin formulation.

The spurious currents also depend on how the curvature is approximated. The exact force balance mentioned above is only achieved when using the exact curvature, which is usually unknown. In many cases, errors in the curvature calculation is the main reason for spurious currents.

The pressure is also affected by how the curvature is approximated. Especially important is how the curvature of the interface is extended into the domain. The best results were obtained when the curvature in points away from the interface was defined as the curvature at the closest point on the interface.

Acknowledgments

The authors gratefully acknowledge discussions with Gustav Amberg, Andreas Carlson, Minh Do-Quang, Anna-Karin Tornberg, and Oana Wiklund. The second author acknowledges collaboration with Bärbel Janssen on time integration. This project has partially been financed by the Graduate School in Mathematics and Computing (FMB), Center for Industrial and applied mathematics at KTH (CIAM), and Linné flow center at KTH. Computations were performed on UPP-MAX and PDC resources.

References

- [1] C. S. Peskin, Numerical Analysis of Blood Flow in the Heart, *J. Comput. Phys.* 25 (1977) 220–252.
- [2] S. O. Unverdi, G. Tryggvason, A Front-Tracking Method for Viscous, Incompressible, Multi-fluid Flows, *J. Comput. Phys.* 100 (1992) 25–37.
- [3] S. Osher, J. A. Sethian, Fronts Propagating with Curvature Dependent Speed: Algorithms Based on Hamilton-Jacobi Formulations, *J. Comput. Phys.* 79 (1988) 12–49.
- [4] C. W. Hirt, B. D. Nichols, Volume of Fluid (VOF) Method for the Dynamics of Free Boundaries, *J. Comput. Phys.* 39 (1981) 201–225.
- [5] D. Jacqmin, Contact-line dynamics of a diffuse fluid interface, *J. Fluid Mech.* 402 (2000) 57–88.

- [6] J. U. Brackbill, D. Kothe, C. Zemach, A continuum method for modeling surface tension, *J. Comput. Phys.* 100 (1992) 335–353.
- [7] Y. C. Chang, T. Y. Hou, B. Merriman, S. Osher, A Level Set Formulation of Eulerian Interface Capturing Methods for Incompressible Fluid Flows, *J. Comput. Phys.* 124 (1996) 449–464.
- [8] A.-K. Tornberg, B. Engquist, Numerical approximations of singular source terms in differential equations, *J. Comput. Phys.* 200 (2004) 462–488.
- [9] S. Zahedi, A.-K. Tornberg, Delta function approximations in level set methods by distance function extension, TRITA-CSC-NA 2009: 1 ISRN KTH/NA-09/01-SE ISSN 0348-2952.
- [10] M. Kang, R. Fedkiw, X. Liu, A boundary condition capturing method for multiphase incompressible flow, *J. Sci. Comput.* 15 (2000) 323–360.
- [11] A.-K. Tornberg, B. Engquist, A Finite Element Based Level Set Method for Multiphase Flow Applications, *Comput. Vis. Sci.* 3 (2000) 93–101.
- [12] B. Lafaurie, C. Nardone, R. Scardovelli, S. Zaleski, G. Zanetti, Modelling merging and fragmentation in multiphase flows with SURFER, *J. Comput. Phys.* 113 (1994) 134–147.
- [13] Y. Renardy, M. Renardy, PROST: A parabolic reconstruction of surface tension for the volume-of-fluid method, *J. Comput. Phys.* 183 (2002) 400–421.
- [14] R. Scardovelli, S. Zaleski, Direct numerical simulation of free-surface and interfacial flow, *Annu Rev: Fluid Mech* 31 (1999) 567–603.
- [15] M. M. Francois, S. J. Cummins, E. D. Dendy, D. B. Kothe, J. M. Sicilian, M. W. Williams, A balanced-force algorithm for continuous and sharp interfacial surface tension models within a volume tracking framework, *J. Comput. Phys.* 213 (2006) 141–173.
- [16] A. Y. Tong, Z. Wang, A numerical method for capillarity-dominant free surface flows, *J. Comput. Phys.* 221 (2007) 506–523.
- [17] S. Popinet, S. Zaleski, A front-tracking algorithm for the accurate representation of surface tension, *Int. J. Numer. Meth. Fluids* 30 (1999) 775–793.
- [18] S. Ganesan, G. Matthies, L. Tobiska, On spurious velocities in incompressible flow problems with interfaces, *Comput. Methods Appl. Mech. Engrg.* 196 (2007) 1193–1202.
- [19] E. Olsson, G. Kreiss, S. Zahedi, A conservative level set method for two phase flow II, *J. Comput. Phys.* 225 (2007) 785–807.

- [20] S. Osher, R. Fedkiw, *Level Set Methods and Dynamic Implicit Surfaces*, Springer-Verlag, 2003.
- [21] J. Sethian, *Level Set Methods and Fast Marching Methods*, Cambridge University Press, 1999.
- [22] D. A. Edwards, H. Brenner, D. T. Wasan, *Interfacial Transport Processes and Rheology*, Butterworth–Heinemann, Stoneham, 1991.
- [23] W. Bangerth, R. Hartmann, K. G., deal.II — a General Purpose Object Oriented Finite Element Library, *ACM Trans. Math. Softw.* 33 (4) (2007) article no. 24.
URL <http://www.dealii.org>
- [24] J. Donea, A. Huerta, *Finite Element Methods for Flow Problems*, J. Wiley & Sons, Chichester, 2003.
- [25] H. Elman, D. Silvester, A. Wathen, *Finite Elements and Fast Iterative Solvers with Applications in Incompressible Fluid Dynamics*, Oxford Science Publications, Oxford, 2005.
- [26] M. Do-Quang, W. Villanueva, G. Amberg, I. Loginova, Parallel adaptive computation of some time-dependent materials-related microstructural problems, *Bull. Polish Acad. Sci.* 55 (2007) 229–237.
- [27] J. L. Guermond, L. Quartapelle, A projection FEM for variable density incompressible flows, *J. Comput. Phys.* 165 (1) (2000) 167–188.
- [28] D. L. Chopp, Some improvements of the fast marching method, *SIAM J. Sci. Comput* 23 (2001) 230–244.
- [29] R. Meland, I. R. Gran, R. Olsen, S. T. Munkejord, Reduction of parasitic currents in level-set calculations with a consistent discretization of the surface-tension force for the CSF model, *16th Australasian Fluid Mechanics Conference* (2007) 862–865.